



## RESEARCH ARTICLE

# Hippocampus shape characterization with 3D Zernike transformation in clinical Alzheimer's disease progression

David C. Zhu<sup>1</sup>  | Chih-Ying Gwo<sup>2</sup>  | An-Wen Deng<sup>2</sup> | Norman Scheel<sup>1</sup> |  
Mari A. Dowling<sup>1</sup> | Rong Zhang<sup>3,4</sup> | for the Alzheimer's Disease Neuroimaging Initiative

<sup>1</sup>Department of Radiology and Cognitive Imaging Research Center, Michigan State University, East Lansing, Michigan, USA

<sup>2</sup>Department of Information Management, Chien Hsin University of Science and Technology, Taoyuan City, Taiwan

<sup>3</sup>Departments of Neurology and Internal Medicine, University of Texas Southwestern Medical Center, Dallas, Texas, USA

<sup>4</sup>Institute for Exercise and Environmental Medicine, Texas Health Presbyterian Hospital Dallas, Dallas, Texas, USA

## Correspondence

David C. Zhu, Department of Radiology, Michigan State University, 846 Service Road, East Lansing, MI 48824, USA.  
Email: zhuda@msu.edu

## Funding information

National Institutes of Health; Department of Defense, Grant/Award Number: W81XWH-12-2-0012; National Institute on Aging, Grant/Award Number: R01AG057571; National Institute of Biomedical Imaging and Bioengineering

## Abstract

Alzheimer's disease (AD) is a neurodegenerative disease and the most common cause of dementia among older adults. Mild cognitive impairment (MCI) is considered a transitional phase between healthy cognitive aging and dementia. Progressive brain volume reduction/atrophy, particularly of the hippocampus, is associated with the transition from normal to MCI, and then to AD. We aimed to develop methods to characterize the shape of hippocampus and explore its potential as an imaging marker to monitor clinical AD progression. We implemented a 3D Zernike transformation to characterize the shape changes of hippocampus in 428 older subjects with high-quality T<sub>1</sub>-weighted volumetric brain scans from the Alzheimer's Disease Neuroimaging Initiative data set (151 normal, 258 MCI, and 19 AD). Over 2 years, 15 cognitively normal subjects converted to MCI, and 42 subjects with MCI converted to AD. We found a significant correlation between hippocampal volume changes and Zernike shape metrics. Before a clinical diagnosis of AD, the shapes of the left and right hippocampi changed slowly. After AD diagnosis, both volume and shape changed rapidly but were uncorrelated to each other. During the transition from a clinical diagnosis of MCI to AD, the shape of the left and right hippocampi changed in a correlated manner but became uncorrelated after AD diagnosis. Finally, the pace of hippocampus shape change was associated with its shape and the subject's age and disease condition. In conclusion, the hippocampus shape features characterized with 3D Zernike transformation, in complement to volume measures, may serve as a novel imaging marker to monitor clinical AD progression.

## KEYWORDS

Alzheimer's disease, hippocampus, shape, Zernike transformation

Data used in the preparation of this article were obtained from the Alzheimer's Disease Neuroimaging Initiative (ADNI) database (adni.loni.usc.edu). As such, the investigators within the ADNI contributed to the design and implementation of ADNI and/or provided data but did not participate in the analysis or writing of this report. A complete listing of ADNI investigators can be found at: [http://adni.loni.usc.edu/wp-content/uploads/how\\_to\\_apply/ADNI\\_Acknowledgement\\_List.pdf](http://adni.loni.usc.edu/wp-content/uploads/how_to_apply/ADNI_Acknowledgement_List.pdf).

David C. Zhu, Chih-Ying Gwo, and Rong Zhang contributed equally to this study.

This is an open access article under the terms of the [Creative Commons Attribution-NonCommercial-NoDerivs](https://creativecommons.org/licenses/by-nc-nd/4.0/) License, which permits use and distribution in any medium, provided the original work is properly cited, the use is non-commercial and no modifications or adaptations are made.

© 2022 The Authors. *Human Brain Mapping* published by Wiley Periodicals LLC.

## 1 | INTRODUCTION

Alzheimer's disease (AD) is a progressive, neurodegenerative brain disorder and the most common cause of dementia among older adults. Patients with AD exhibit a gradual decline in cognitive function, resulting in memory loss, impaired decision-making capacity, disorientation, as well as changes in personality and mood (McKhann et al., 2011). The cognitive decline and behavioral changes are accompanied by histological changes including neuronal degeneration and abnormal protein deposition in the cerebral cortex (Querfurth & LaFerla, 2010). Mild cognitive impairment (MCI) is a clinical syndrome considered to represent a transitional phase between healthy cognitive aging and dementia (Petersen et al., 1999). In contrast to dementia, cognitive deficits observed in patients with MCI are milder and typically do not interfere with an individual's ability to perform activities of daily living. Importantly, patients with MCI have a significantly increased risk of developing dementia, with a 10%–15% annual rate of progression (Petersen et al., 2009). Identifying the characteristics of the sub-population of MCI individuals who are at a higher risk of converting to AD is critical for preventative and treatment interventions.

Global and regional brain volume loss has been found to be associated with disease progression from normal cognition to MCI, and then to AD. Among the various brain regions, hippocampus volume reduction was found to be a sensitive and reliable imaging biomarker to monitor clinical AD progression (Jack et al., 1999, 2004, 2005). The current characterization of hippocampus changes has mostly been limited to volumetric analysis. Nevertheless, the hippocampus contains multiple subfields, with the subiculum and CA1 changes likely associated with AD pathophysiology, and the CA3 and dentate gyrus changes associated with normal aging (Jagust, 2013; Pievani et al., 2011). Given these region-specific differences in the underlying neurobiological mechanisms, it is reasonable to speculate that the hippocampus may undergo both volumetric and shape changes corresponding to normal aging and the stage of clinical AD progression. Prior work by Wachinger et al. has demonstrated a significant increase in hippocampus left–right asymmetry in dementia (Wachinger et al., 2016). Therefore, analysis of changes in hippocampus shape, in complement to volume measures, may contribute to the understanding of the dynamics of hippocampus volume loss and possibly serve as a novel image marker for AD.

In this regard, Wachinger et al. (2016) utilized a statistical shape analysis method developed by Styner et al. (2006) to characterize hippocampus shape features in dementia. This method is based on spherical harmonics analysis of an object's shape. Spherical harmonics analysis can be used to characterize a shape with a spherical topology, but it would fail to characterize complicated shapes, such as structures with holes and tori (Venkatraman et al., 2009).

Brain structures contain complex shapes, with various curvatures, extensions, and pockets in the brain's gyri and sulci. To fully characterize complicated shape features such as the brain structures, the applied methodology must be able to characterize topological structures with holes and tori. The methods should also have properties such as spatial invariants to the object orientations, resistance to image noise, and being able to define a one-to-one mapping

relationship between the object shape and shape feature vectors. Zernike transformation can satisfy these criteria (Khotanzad & Hong, 1990). Similar to the Fourier analysis, the shape features of an object captured on MRI can be represented by the coefficients of the Zernike polynomial expansion (i.e., Zernike transformation), referred to as Zernike moments (ZMs) (Zernike, 1934). Recently, we applied a 2D version of Zernike transformation to characterize  $T_2$  FLAIR white-matter hyperintensity brain lesions in cognitively normal older adults (Gwo et al., 2019). We were able to characterize white matter hyperintensity brain lesions to six distinct shape clusters, which were significantly correlated with a lesion growth index calculated based on the border characteristics of the white matter lesions. These observations suggest that longitudinal changes of brain white matter lesions may be influenced by their shape characteristics. We now explore the application of 3D Zernike transformation to characterize hippocampus shape changes related to clinical AD progression. First, we aim to demonstrate the applicability of 3D Zernike transformations to characterize hippocampus shape features. Second, we aim to evaluate hippocampus shape changes over the time course of clinical AD progression, as well as their relationships with hippocampus volume changes.

## 2 | METHODS

### 2.1 | 3D Zernike transformation

The 2D Zernike transformation is based on the Zernike polynomials defined on a unit disc  $D$ . It has been used extensively in imaging shape feature extraction and pattern recognition (Gwo et al., 2019; Papakostas et al., 2007; Wee & Paramesran, 2007). The coefficients of the Zernike polynomial expansion of an object are called ZMs. ZMs are complex numbers. The magnitude of ZM is rotationally invariant and represents the shape features of the objects being analyzed. To define the 3D version of Zernike polynomials, the unit disc  $D$  is replaced by a unit ball  $B$ . Every point  $(x, y, z)$  in the unit ball  $B$  can be represented by a spherical coordinate  $(r, \theta, \phi)$  as shown in Equation (1),

$$(x, y, z) = (r \sin \theta \cos \phi, r \sin \theta \sin \phi, r \cos \theta). \quad (1)$$

where

$$\begin{aligned} r &= \sqrt{x^2 + y^2 + z^2}, \\ \theta &= \cos^{-1} \frac{z}{r}, \\ \phi &= \sin^{-1} \frac{y}{\sqrt{x^2 + y^2}}. \end{aligned} \quad (2)$$

Canterakis introduced the first algorithm to calculate 3D Zernike moments (3DZMs) (Canterakis, 1999), where the 3DZMs were expressed as the linear combination of geometric moments. These

3DZMs were later described as shape descriptors for shape retrieval (Novotni & Klein, 2004). Canterakis' algorithm has been applied to terrain matching (Wang et al., 2018, 2019) and protein-protein interface prediction (Daberduku & Ferrari, 2018). However, Canterakis' algorithm could only be used to compute ZM up to the order of 25, due to computational demand and instability. Hosny et al. introduced a fast algorithm using eight ways of (anti-)symmetries (Hosny & Hafez, 2012). To overcome the limitations on computational efficiency and the maximum ZM order that can be computed reliably in previous algorithms, Deng & Gwo proposed a new algorithm based on a recursive approach to calculate 3D Zernike radial polynomials (Deng & Gwo, 2020). This full algorithm to calculate the 3D Zernike polynomial is described below.

The 3D Zernike polynomial  $V_{n\ell}^m(r, \theta, \phi)$  is defined as the multiplication of spherical harmonic  $Y_{\ell}^m(\theta, \phi)$  and radial polynomial  $R_{n\ell}(r)$  as below:

$$V_{n\ell}^m(r, \theta, \phi) = Y_{\ell}^m(\theta, \phi)R_{n\ell}(r). \quad (3)$$

$Y_{\ell}^m(\theta, \phi)$  and  $R_{n\ell}(r)$  are computed separately. The spherical harmonic  $Y_{\ell}^m(\theta, \phi)$  of degree  $\ell$  with order  $m$  is given by

$$Y_{\ell}^m(\theta, \phi) = \begin{cases} K_{\ell}^m P_{\ell}^m(\cos\theta) \cos m\phi & \text{if } m \geq 0 \\ K_{\ell}^m P_{\ell}^m(\cos\theta) \sin m\phi & \text{otherwise} \end{cases} \quad (4)$$

where  $P_{\ell}^m(\cdot)$  is the associated Legendre polynomial of degree  $\ell$ , given by

$$P_{\ell}^m(x) = (-1)^m (1-x^2)^{\frac{m}{2}} \frac{d^m}{dx^m} (P_{\ell}(x)). \quad (5)$$

and  $K_{\ell}^m$  is the normalizing factor given by

$$K_{\ell}^m = (-1)^m \sqrt{\frac{\epsilon_m (2\ell+1)(\ell-m)!}{(\ell+m)!}} \text{ Where } \epsilon_m = \begin{cases} 1 & \text{if } m \neq 0 \\ 2 & \text{otherwise} \end{cases} \quad (6)$$

Let  $\tilde{P}_{\ell}^m(\cos\theta) = K_{\ell}^m P_{\ell}^m(\cos\theta)$  be the normalized associated Legendre polynomial, then Equation (4) is simplified to

$$Y_{\ell}^m(\theta, \phi) = \begin{cases} \tilde{P}_{\ell}^m(\cos\theta) \cos m\phi & \text{if } m \geq 0 \\ \tilde{P}_{\ell}^m(\cos\theta) \sin m\phi & \text{otherwise} \end{cases} \quad (7)$$

The spherical harmonics  $Y_{\ell}^m(\cdot)$  form an orthonormal basis for the Hilbert space  $L^2(S^2)$  of the square-integrable functions over the unit sphere  $S^2$ . For any function  $f$  in  $L^2(S^2)$ ,  $f$  can be expressed as in Equation (8) (Szegő, 1939):

$$f(\theta, \phi) = \sum_{\ell=0}^{\infty} \sum_{m=-\ell}^{\ell} C_{\ell}^m Y_{\ell}^m(\theta, \phi), \quad (8)$$

where  $C_{\ell}^m$  are the coefficients;  $\ell$  is a nonnegative integer;  $m$  is an integer with  $|m| \leq \ell$ . The computation procedures of  $\tilde{P}_{\ell}^m(\cos\theta)$  for degree

$\ell \leq \ell_{max}$  are summarized as follows (Deng & Gwo, 2018; Szegő, 1939):

1. Initialize  $\tilde{P}_0^0(\cos\theta) = \sqrt{\frac{1}{4\pi}}$ , which is the normalizing factor for volumetric integration. Then iteratively calculate the following:
2.  $\tilde{P}_{\ell}^m(\cos\theta) = C_3 \sin\theta P_{\ell-1}^{m-1}(\cos\theta)$  for  $\ell = 1, 2, 3, \dots, \ell_{max}$

$$P_{\ell}^{\ell-1}(\cos\theta) = C_1 \cos\theta P_{\ell-1}^{\ell-1}(\cos\theta)$$

$$\tilde{P}_{\ell}^m(\cos\theta) = C_1 \cos\theta P_{\ell-1}^m(\cos\theta) - C_2 P_{\ell-2}^m(\cos\theta)$$

for  $m = 0, 1, \dots, \ell - 2$

$$C = \sqrt{\frac{2\ell+1}{(\ell+m)(\ell-m)}}, C_1 = C\sqrt{2\ell-1}$$

$$C_2 = C\sqrt{\frac{(\ell+m-1)(\ell-m-1)}{2\ell-3}}, C_3 = \sqrt{\frac{2\ell+1}{2\ell}}. \quad (9)$$

For a Zernike polynomial of order  $n$  (a nonnegative integer), the integer  $\ell$  above needs to be  $\leq n$  and  $n - \ell = \text{even}$ , while the integer  $m$  needs to satisfy  $|m| \leq \ell$ . The 3D Zernike radial polynomial  $R_{n\ell}(r)$  in Equation (3) was originally given in terms of Jacobi polynomials as described in (Szegő, 1939), but different calculation methods of 3D Zernike radial polynomial have been proposed (Deng & Gwo, 2020). In our work,  $R_{n\ell}$  is computed recursively, similar to Kintner's  $p$ -method in the case of 2D Zernike polynomials, shown in Equation (10) (Deng & Gwo, 2018; Kintner, 1976). Here, the reconstruction error of ZMs for orders greater than 20 is much smaller than that using Canterakis' method based on geometric moments.

$$R_{n\ell}(r) = (K_1 r^2 + K_2) R_{n-2, \ell}(r) + K_3 R_{n-4, \ell}(r), \quad (10)$$

for  $n = \ell + 4, \ell + 6, \dots, n_{max}$

where the coefficients  $K_i$  are given by the following,

$$\kappa_0 = (n-\ell)(n+\ell+1)(2n-3),$$

$$\kappa_1 = (2n-1)(2n+1)(2n-3),$$

$$\kappa_2 = (-2n+1) \left( \frac{4\ell^2 + 4\ell + 1}{2} \right) - \frac{\kappa_1}{2},$$

$$\kappa_3 = -(n-\ell-2)(n+\ell+1)(2n+1),$$

$$K_1 = \frac{\kappa_1}{\kappa_0}, K_2 = \frac{\kappa_2}{\kappa_0}, K_3 = \frac{\kappa_3}{\kappa_0}. \quad (11)$$

For this recursive formula, the following initial equalities are also required:

$$R_{nm}(r) = r^n \text{ for } n = 0, 1, 2, \dots, \quad (12)$$

and

$$R_{n,n-2}(r) = \left(n + \frac{1}{2}\right)r^n - \left(n - \frac{1}{2}\right)r^{n-2} \text{ for } n = 2, 3, 4, \dots \quad (13)$$

Let  $f(r, \theta, \phi)$  be a 3D image function within the unit ball  $B$ . The 3DZM  $Z_{n\ell}^m$  can be rationalized as the inner product of the image function  $f(r, \theta, \phi)$  and the basis function  $V_{n\ell}^m(r, \theta, \phi)$  (Deng & Gwo, 2020), and can be described as

$$Z_{n\ell}^m = (2n + 3) \int\int\int_{(r, \theta, \phi) \in B} f(r, \theta, \phi) V_{n\ell}^m(r, \theta, \phi) r^2 \sin \theta dr d\theta d\phi. \quad (14)$$

Each moment within Order  $n$  corresponds to a  $(2\ell + 1)$ -dimensional vector

$$\vec{Z}_{n\ell} \quad (as) \quad (15)$$

$$\vec{Z}_{n\ell} = \left( Z_{n\ell}^{-\ell}, Z_{n\ell}^{-\ell+1}, \dots, Z_{n\ell}^0, \dots, Z_{n\ell}^{\ell-1}, Z_{n\ell}^{\ell} \right). \quad (15)$$

The  $l^2$ -norm of  $\vec{Z}_{n\ell}$ , denoted by

$$\|\vec{Z}_{n\ell}\| = \sqrt{\sum_{m=-\ell}^{\ell} |Z_{n\ell}^m|^2}, \quad (16)$$

is rotationally invariant and can be used as the 3D shape descriptor (or Zernike descriptor) of a 3D object. The total number of 3DZMs and the dimension of the Zernike descriptor for an expansion up to order  $n$  are given by Equation (17) and Equation (18) respectively:

$$\text{Number of 3DZMs} = \sum_{i=0}^n \left\lfloor \frac{(i+2)^2}{4} \right\rfloor. \quad (17)$$

$$\text{Dimension of Zernike descriptor} = \begin{cases} \frac{\left(\frac{n+2}{2}\right)^2}{4} & \text{if order } n \text{ is even} \\ \frac{(n+3)(n+1)}{4} & \text{if order } n \text{ is odd} \end{cases} \quad (18)$$

The image object function  $f$  can be reconstructed with ZM order  $M$  as  $f_M$  below:

$$f_M(r, \theta, \phi) = \sum_{n=0}^M \sum_{\ell} \sum_{m=-\ell}^{\ell} Z_{n\ell}^m V_{n\ell}^m(r, \theta, \phi). \quad (19)$$

When  $M$  is large enough, the function  $f_M$  can be used to approximate the original image object function  $f$  (Deng & Gwo, 2018). For a binary image object with the background represented by 0, the error rate  $\mathcal{E}_r$  between the original  $f$  and the reconstructed  $f_M$  can be calculated by

$$\mathcal{E}_r = \frac{\sum_{\forall(x, y, z)} (f(x, y, z) \oplus f_M(x, y, z))}{\sum_{\forall(x, y, z)} f(x, y, z)},$$

$$\text{where } f_M(x, y, z) = \begin{cases} 1 & \text{if } f_M(x, y, z) \geq 0.5 \\ 0 & \text{otherwise} \end{cases}. \quad (20)$$

where  $\oplus$  is exclusive disjunction and  $f(x, y, z) = 0$  or 1. Based on the error rate  $\mathcal{E}_r$ , an appropriate ZM order  $M$  can be chosen.

Overall, the calculation of 3DZMs is summarized as following: First, the normalized associated polynomial  $\tilde{P}_{\ell}^m(\cos \theta)$  of the spherical harmonic function is calculated using Equation (9). Second, the 3D Zernike radial polynomial  $R_{n\ell}$  is calculated recursively using Equations (10)–(13). Then, the 3D Zernike polynomials can be obtained by Equation (3). Finally, Equation (14) is used to generate 3DZMs, and Equation (16) is used to generate the 3D Zernike descriptors. The 3D spherical harmonics and Radial polynomials are illustrated in Figure 1.

The applicability of 3D Zernike descriptors to characterize the shape of brain structures can be illustrated with the left and right hippocampi and the right lateral occipital cortex (Figure 2a). In Figure 2a, these three brain structures have been normalized to the same size. The corresponding Zernike descriptors are plotted in Figure 2b. As shown in Figure 2b, the magnitudes of Zernike descriptors of the left and right hippocampi are nearly overlaid with each other in most descriptor indices, but are notably different from those of the right lateral occipital cortex, as expected.

## 2.2 | Subjects

Subjects who had at least 2 years of anatomical MRI data were selected from the Alzheimer's Disease Neuroimaging Initiative (ADNI) database (<http://adni.loni.usc.edu/>), resulting in 521 subjects when we started this study. High-resolution whole-brain  $T_1$ -weighted 3D MR images of these subjects were used for this study.  $T_1$ -weighted 3D MR images were acquired with a full-brain sagittal 3D IRFSPGR (inversion recovery fast spoiled gradient-recalled) protocol on a 3T GE scanner, or a sagittal 3D MPRAGE (magnetization prepared rapid acquisition gradient recalled echo) protocol on a 3T Siemens or Philips scanner with a voxel resolution of  $1 \times 1 \times 1.2 \text{ mm}^3$ . All  $T_1$ -weighted volumetric images were processed through the FreeSurfer segmentation pipeline (Fischl et al., 2002). In this pipeline, the  $T_1$ -weighted 3D MR images were normalized to have a voxel size of  $1 \times 1 \times 1 \text{ mm}^3$  and a voxel signal intensity range of 0–255. The left and right hippocampi were segmented along with other brain regions. Subjects exhibited significant motion artifacts often resulted in image segmentation failure. All images and segmentation results were visually inspected by a trained research assistant to ensure quality. Images with bad segmentation quality were excluded from this study, resulting in a total of 2683 high-quality  $T_1$ -weighted 3D MR images available for analysis. While the original data set contained 521 subjects in total, only those who had high-quality  $T_1$ -weighted 3D MR images at both baseline and 24-month follow-up scans were included for statistical

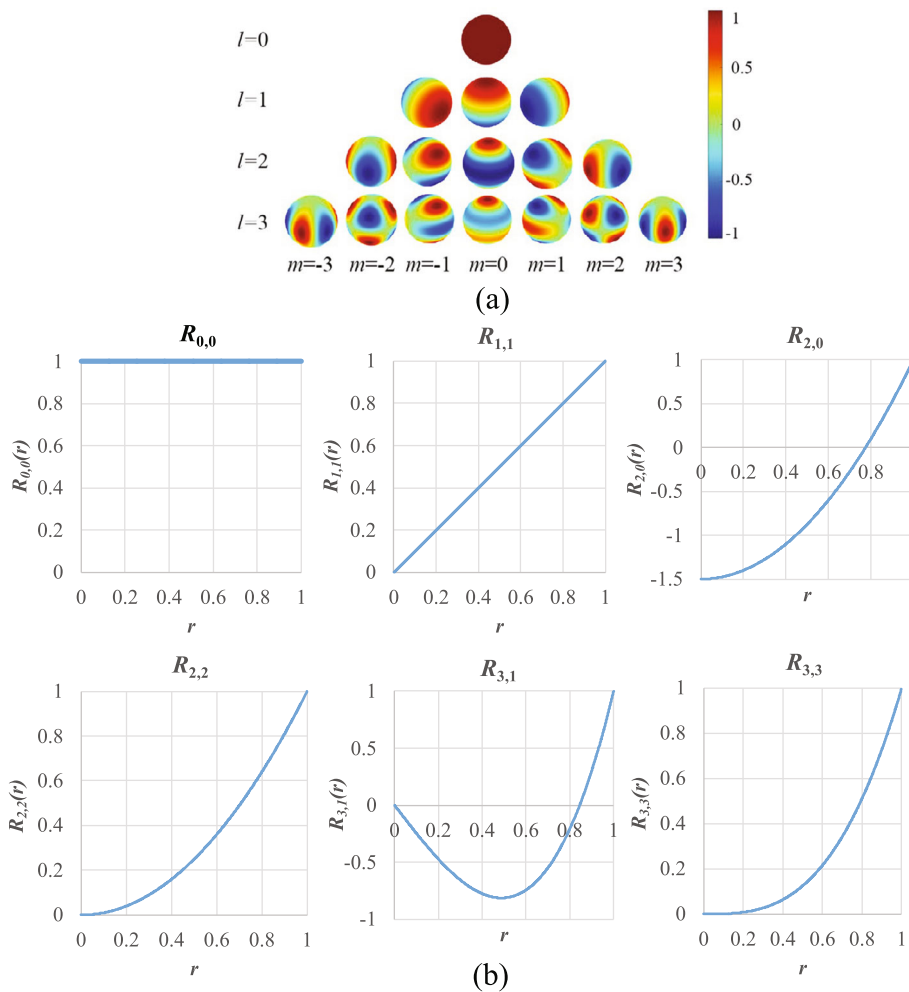


**FIGURE 1** (a) Spherical harmonics  $Y_l^m(\theta, \phi)$  of different degree  $l$  with order  $m$  from  $-l$  to  $l$  are shown with image from @2021 IEEE. Reprinted, with permission, from Liu et al. (2019). (b) The radial polynomials for order  $n = 0, 1, 2,$  and  $3$  are illustrated

analyses. In addition, only two subjects changed from normal cognition to dementia within a time window of 2 years investigated in this study. Thus, a category of conversion from normal aging to dementia was not included in this study due to the lack of statistical power. The total number of subjects included for statistical analysis was 428. Based on the cognitive conditions assessed at baseline (Month 0) and Month 24, subjects were divided into the following groups: Normal–Normal cognition (N–N), Normal cognition–MCI (N–M), MCI–Normal cognition (M–N), MCI–MCI (M–M), MCI–Dementia (M–D), Dementia–Dementia (D–D) (Table 1). Table 1 also includes ApoE4 status, Mini-Mental State Examination score, and brain amyloid level measured via AV45 PET scan, as well as TAU and PTAU concentrations measured in cerebrospinal fluid (CSF).

### 2.3 | Hippocampus shape normalization and template generation

To compare the differences and changes in shapes of either the left or right hippocampi of the subjects, the hippocampi need to be uniformly resampled to a common size, logically, the approximate median size of 4000 voxels (voxel size =  $1 \text{ mm}^3$ ) in this work. The median size of the left hippocampi of these subjects was found to be 3746 voxels, and

that of the right hippocampi was 3954 voxels. The following procedure was applied to the left hippocampus and then repeated on the right.

After resizing to 4000 voxels, a common reference template was first created to compare with the hippocampus shape of an individual subject. Specifically, this template was generated using an iterative closest point (ICP) algorithm, integrating the hippocampus images from the high-quality  $T_1$ -weighted 3D MR images (total of 2683) from the original 521 subjects. In the ICP algorithm, the source image is transformed to match the reference image with 6-degree affine rigid-body transformation. The algorithm iteratively minimizes the sum of the distances of the source and reference point pairs, to achieve the best match between two sets of data points. ICP is widely used for aligning three-dimensional rigid shapes (Besl & McKay, 1992; Chen & Medioni, 1992). After the boundary points of all resized hippocampi from all subjects were identified, the hippocampus template (the left and then the right one) was generated using the following steps:

Step 1: Initialize one resized hippocampus (at the common pre-defined 4000-voxel size) from a subject as the reference template.

Step 2: Match the boundary points of another resized hippocampus to the template based on the ICP algorithm and generate the

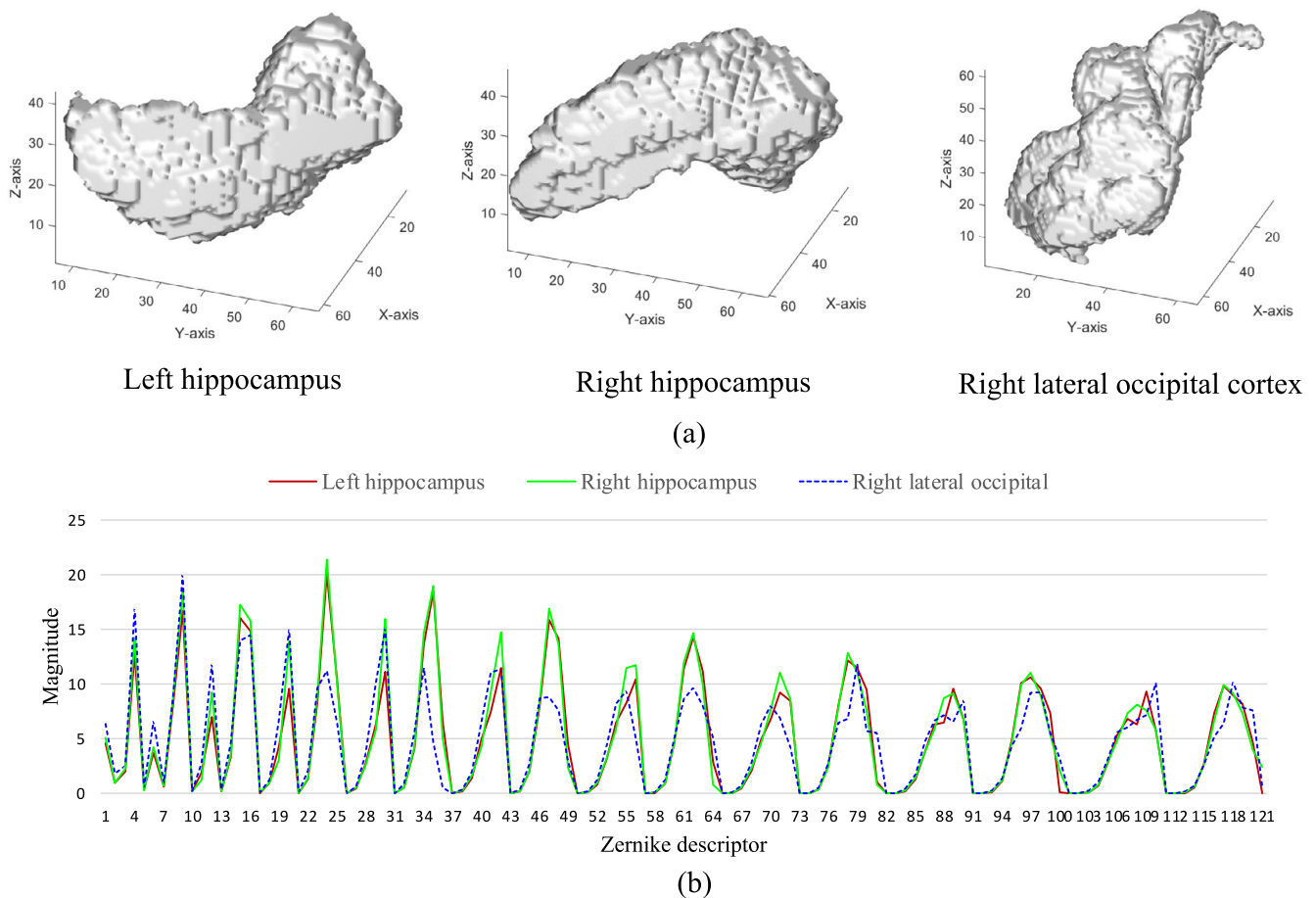


**FIGURE 2** (a) Three 3D brain structures (left hippocampus, right hippocampus and right lateral occipital cortex) were normalized to fit in the cube of  $70 \times 70 \times 70$  voxels. (b) The magnitudes of 121 Zernike descriptors based on Zernike moment orders  $\leq 20$  of these three structures are shown for comparison.

6-degree affine transformation matrix. Align this resized hippocampus to the template based on this transformation matrix.

Step 3: Repeat Step 2 to all resized individual hippocampus.

Step 4: After Step 3, all resized hippocampi have been aligned to a common template. The average voxel signal intensity across the resized hippocampi would produce the mean image with voxel intensity values between 0 and 255.

Step 5: To generate a binary map to represent the hippocampus shape, a threshold of 128 signal intensity is applied to the mean image generated from Step 4. However, since the image size becomes deviated from the pre-defined 4000-voxel volume size, the average image volume is resized again to the 4000-voxel volume size as the last step to generate the final template. This final template contains a smooth boundary and represents the whole group (Figure S1).

## 2.4 | Shape feature extraction

To compute the 3DZMs of the hippocampus, a ZM order needs to be determined. This decision can be based on the relationship between

ZM order and reconstruction error rate, described in Equation (20). For the left hippocampus of a subject shown in Figure 3a, at a low ZM order, such as 40, the error rate is high and a significant amount of image details is missing. At a high ZM order, such as 200 in this example, the error rate is low, and the reconstructed image looks similar to the original image. A wide range of ZM orders can be used, depending on the desired threshold of the error rate (Figure 3b). In this work, we chose a ZM order of 200. At this ZM order, the reconstruction error rates of the left and right hippocampi of this subject approach the plateau of zero (Figure 3b). At this ZM order, the reconstruction error rates of the left and right hippocampi of all 428 subjects at baseline were  $(2.18 \pm 0.60) \times 10^{-2}$  and  $(2.19 \pm 0.56) \times 10^{-2}$ , respectively. The ZM order of 200 led to a Zernike descriptor with 10,201 dimensions. To improve computational efficiency, principal component analysis (PCA) was applied to reduce the high dimensions associated with the Zernike descriptor. To compute the principal components in an unbiased manner, the Zernike descriptors of the hippocampi of the high-quality  $T_1$ -weighted 3D MR images (total of 2683) from the original 521 subjects were combined to generate a covariance matrix, from which the eigenvectors and eigenvalues were estimated. The eigenvectors corresponding to the 120 largest eigenvalues (expected to

TABLE 1 Subject demographics

Group <sup>a</sup>		N-N	N-M	M-N	M-M	M-D	D-D
# of Subjects (Total: 428)		136	15	10	206	42	19
(F, M)		(67, 69)	(9, 6)	(6, 4)	(89, 117)	(21, 21)	(9, 10)
Age		72.4 ± 6.2	75.3 ± 6.5	68.7 ± 5.6	70.7 ± 7.3	71.1 ± 7.4	75.7 ± 9.0
ApoE4 status	0	97 (71.3%)	10 (66.7%)	7 (70.0%)	119 (57.8%)	11 (26.2%)	4 (21.1%)
(# of subjects and %)	1	37 (27.2%)	4 (26.7%)	3 (30%)	69 (33.5%)	23 (54.8%)	12 (63.2%)
	2	2 (1.5%)	1 (6.7%)	0 (0%)	18 (8.7%)	8 (19.0%)	3 (15.8%)
MMSE score	Baseline	29.1 ± 1.2	28.7 ± 0.9	29.2 ± 0.4	28.4 ± 1.6	26.8 ± 1.7	22.5 ± 1.5
	Month 24	29.1 ± 1.2	28.0 ± 1.6	29.7 ± 0.9	28.0 ± 2.1 (3)	23.8 ± 3.2	17.4 ± 4.4
Brain amyloid (SUVR)	Baseline	1.09 ± 0.17	1.19 ± 0.19	1.12 ± 0.12	1.14 ± 0.18 (1)	1.43 ± 0.19	1.43 ± 0.24
	Month 24	1.12 ± 0.22 (12)	1.17 ± 0.19 (3)	1.13 ± 0.15 (1)	1.16 ± 0.20 (34)	1.43 ± 0.19 (2)	1.43 ± 0.25 (2)
CSF TAU (pg/ml)	Baseline	245.1 ± 93.3 (15)	250.1 ± 90.0 (2)	211.0 ± 50.9 (2)	256.2 ± 120.4 (15)	387.4 ± 156.0	420.1 ± 124.2
	Month 24	250.4 ± 101.6 (58)	289.8 ± 114.0 (9)	268.5 ± 57.4 (6)	287.4 ± 133.8 (92)	443.5 ± 180.2 (18)	420.3 ± 128.0 (10)
CSF PTAU (pg/ml)	Baseline	22.3 ± 9.3 (16)	22.7 ± 9.0 (2)	19.1 ± 5.1 (2)	24.0 ± 13.2 (15)	39.4 ± 17.5	42.5 ± 13.0
	Month 24	23.3 ± 11.0 (59)	27.5 ± 12.3 (9)	26.3 ± 5.5 (6)	27.3 ± 15.1 (93)	44.0 ± 19.8 (18)	42.0 ± 13.3 (10)

Note: ApoE4 status: Carrier of 0, 1, or 2 ApoE4 alleles.

Brain amyloid: Average AV45 SUVR of frontal, anterior cingulate, precuneus, and parietal cortex relative to the cerebellum.

CSF TAU and PTAU: TAU and PTAU proteins measured in CSF.

Brain amyloid, CSF TAU, and CSF PTAU: The numbers of missing data are indicated in parentheses.

Abbreviations: CSF, cerebrospinal fluid; D, dementia; M, mild cognitively impaired; MMSE, Mini-Mental State Examination; N, normal cognition.

<sup>a</sup>Group shows the cognitive condition changed from baseline to Month 24.

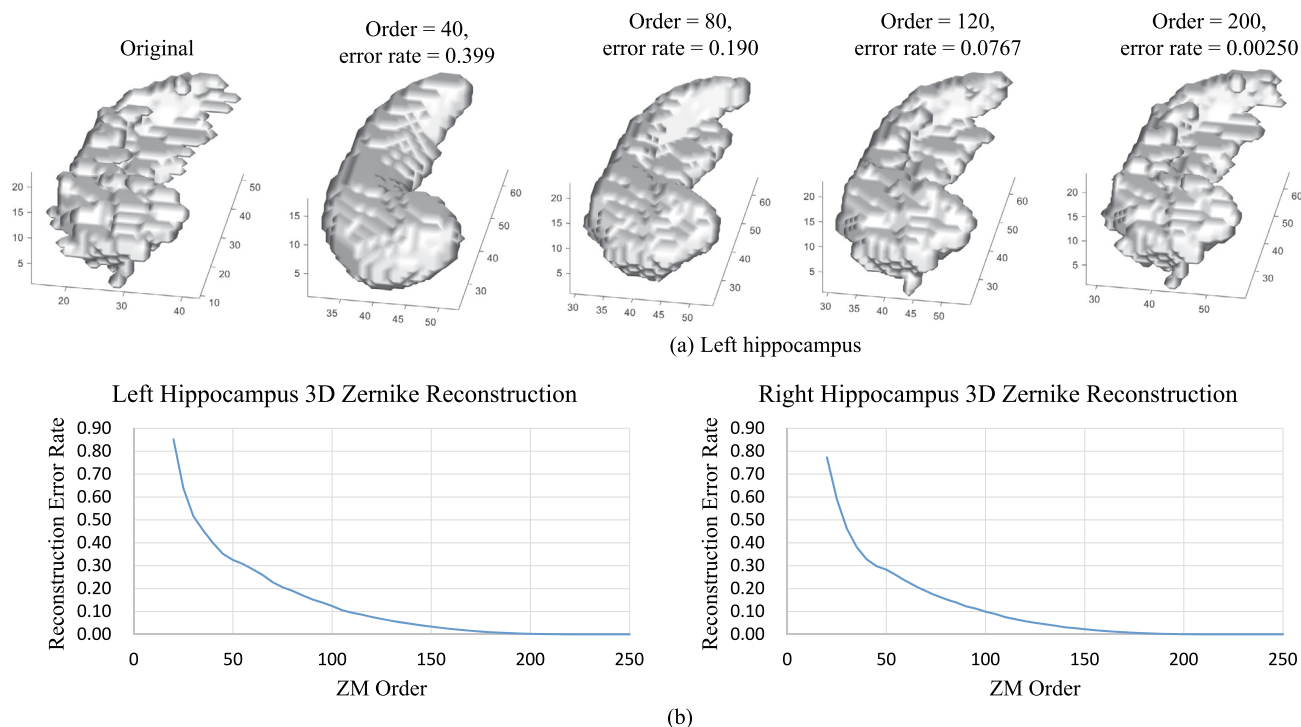


**FIGURE 3** Top-row images (a) illustrate the effects of back transformations at the Zernike moment (ZM) orders of 40, 80, 120, and 200 for the left hippocampus of a subject. The error rates are indicated. Bottom-row plots (b) show the reconstruction error rates of this subject's two hippocampi at different ZM orders. When the ZM order = 200, the error rates of the left and right hippocampi are  $2.50 \times 10^{-2}$  and  $7.51 \times 10^{-4}$ , respectively

contain >89% of the total accumulative variance) were selected as the principal components to compose the transformation matrix. The original 10,201-dimension Zernike descriptor of the hippocampus of each subject or the template was then projected to the 120 principal eigenvectors via this transformation matrix. Then the Euclidean distance  $S_M(x)$  at Month  $M$  (0 or 24) between the hippocampus Zernike descriptor  $x$  of a subject after dimensionality reduction and the Zernike descriptor  $\mu$  of the template after dimensionality reduction is calculated as

$$S_M(x) = \sqrt{(x-\mu)^T(x-\mu)}.$$

The shape change from the baseline over 24 months can be quantified as  $dS_{24} = S_{24} - S_0$ . The corresponding hippocampus volume change is  $dV_{24} = V_{24} - V_0$ .

## 2.5 | Statistical analyses

The percentages of changes in hippocampus shape and volume for each group were calculated, and the shape and volume change distributions were assessed. The Pearson correlations between the changes in shape and volume of the hippocampus overall as well as in each group were calculated. The Pearson correlations between the baseline brain amyloid level (and similarly baseline CSF TAU and PTAU concentrations) and the shape change of the hippocampus over 24 months overall as well as in each group were calculated. The Pearson correlations between the shapes of the left and right hippocampi at baseline and Month 24, as well as their changes over 24 months, were also calculated. A two-way ANOVA was applied to

assess whether there were significant shape changes over 24 months and interactions between different groups. In addition, ANCOVA was applied to reveal whether shape changes over 24 months were influenced by the baseline shape measures, group category, age, sex, ApoE4 status (negative and positive), baseline brain amyloid level, and baseline CSF TAU and PTAU concentrations. Each noncategory input was first normalized to the range of 0–1 based on its min–max range. Linear model fits were then examined with the residual analysis lme4 (version 1.1-27.1) package for statistical computing environment R (version 3.6.3). Due to the small number of subjects in Groups N–M ( $n = 15$ ) and M–N ( $n = 10$ ), only the N–N, M–M, M–D, D–D groups were included in the ANOVA and ANCOVA analyses.

## 3 | RESULTS

The data analyses include 428 older adults with high-quality brain  $T_1$ -weighted 3D MR images at both baseline and 24 months, including subjects with normal cognition (N), mild cognitive impairment (M or MCI), and dementia (D or AD). Most subjects are in Groups N–N and M–M (Table 1). Table 2 shows the percentage changes in hippocampus shape and volume for each group and overall over 24 months, as well as the correlation between the changes in shape and volume. The highest % changes in both volume and shape occurred in the M–D and D–D groups. There were overall significant correlations ( $r = -.483$  for the left and  $r = -.298$  for the right) between hippocampus shape and volume changes. However, the significant correlations only extended to the N–N and M–M groups, and partially to the M–N group. The relationship between the shape and volume changes for each group is illustrated in the scatter plots shown in Figures S3

**TABLE 2** Hippocampus shape and volume % changes over 24 months and correlations between their changes

Group	Shape change ( $dS_{24}$ ) %		Volume change ( $dV_{24}$ ) %		$r(dS_{24}\%, dV_{24}\%), p, CI_{0.95}$	
	Left	Right	Left	Right	Left	Right
N–N <sup>a</sup>	1.54 ± 12.20	1.79 ± 13.92	−2.50 ± 5.21	−2.49 ± 6.90	−0.414, $5.52 \times 10^{-7}$ , [−0.610, −0.270]	−0.397, $1.76 \times 10^{-6}$ , [−0.590, −0.250]
N–M	4.44 ± 10.70	4.26 ± 8.42	−3.46 ± 5.78	−3.49 ± 4.65	−0.480, .070, [−1.089, 0.042]	0.264, .342, [−0.296, 0.836]
M–N	12.62 ± 42.76	−3.51 ± 10.77	−9.05 ± 17.16	−1.01 ± 4.44	−0.931, $8.98 \times 10^{-5}$ , [−2.409, −0.927]	−0.161, .657, [−0.903, 0.579]
M–M <sup>a</sup>	2.35 ± 11.49	2.23 ± 11.69	−3.28 ± 7.31	−2.66 ± 7.45	−0.288, $2.70 \times 10^{-5}$ , [−0.434, −0.159]	−0.235, $6.87 \times 10^{-4}$ , [−0.377, −0.102]
M–D	7.53 ± 12.09	6.46 ± 11.84	−7.99 ± 6.02	−8.46 ± 5.98	−0.246, .117, [−0.564, 0.063]	−0.129, .416, [−0.443, 0.184]
D–D	10.04 ± 12.82	2.96 ± 13.26	−8.79 ± 8.45	−9.12 ± 6.31	−0.305, .204, [−0.805, 0.174]	−0.337, .158, [−0.841, 0.139]
Overall <sup>a</sup>	3.25 ± 13.66	2.47 ± 12.52	−3.88 ± 7.30	−3.45 ± 7.28	−0.483, $2.19 \times 10^{-26}$ , [−0.622, −0.432]	−0.298, $3.32 \times 10^{-10}$ , [0.402, 0.212]

Note:  $r$  = the correlation coefficient between  $dS_{24}\%$  and  $dV_{24}\%$ .

$CI_{0.95}$  denotes the 95% confidence interval on the Fisher's  $Z$  value of  $r$ .

<sup>a</sup>Group with significant correlations observed in both left and right hippocampi.



and S4. Different groups changed their hippocampus shapes in different patterns (Figure 4). The N-N and M-M groups tended to shrink in the central region. The M-D and D-D groups tended to enlarge at the tails but also shrink in the central region. The shape change distributions are shown in Figure 5. The M-D and D-D groups show the highest changes in shape. The volume changes for different groups are illustrated in Figure S2. The M-D and D-D groups show the highest decreases in volume.

Overall significant correlations between the baseline brain amyloid level and shape change over 24 months were found ( $r = .106$  and  $p = .029$  for the left and  $r = .098$  and  $p = .043$  for the right), but not within individual groups. Significant correlations between CSF TAU/PTAU concentration and the shape change were not found.

Significant overall correlations between the shape characteristics of the left and right hippocampi were found at both baseline and Month 24 (Table 3). Significant correlations were also found in Groups of N-N, M-M, and M-D, and partially in D-D. The overall correlations between the shape changes of the left and right hippocampi over 24 months were significant. These significant correlations in shape changes were found in Groups M-M and M-D (Table 3, Figure S5).

ANOVA showed significant group differences on the shape changes over 24 months for the left hippocampus ( $p = 2.24 \times 10^{-5}$ ) and approaching significance for the right hippocampus ( $p = 5.20 \times 10^{-2}$ ). Significant differences were found between most group pairs for the left hippocampus, except between Groups N-N

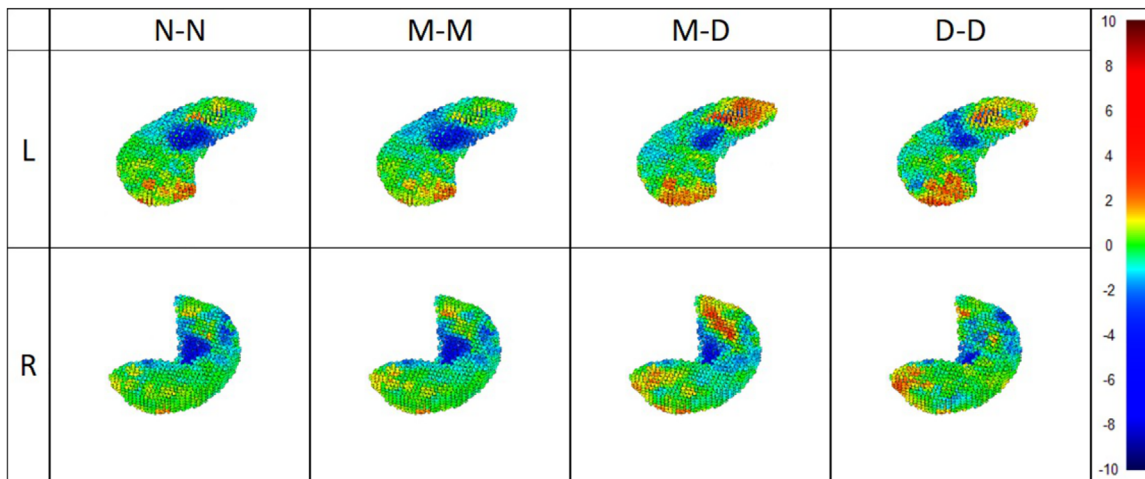


**FIGURE 4** The regions affected over 24 months can be visualized via color coding on the mean left (L) and right (R) hippocampi for different groups. The color coding shows changes from the centroids in mm. Groups are categorized by the changes of cognitive conditions over 24 months with N = normal, M = mild cognitive impairment, and D = dementia.

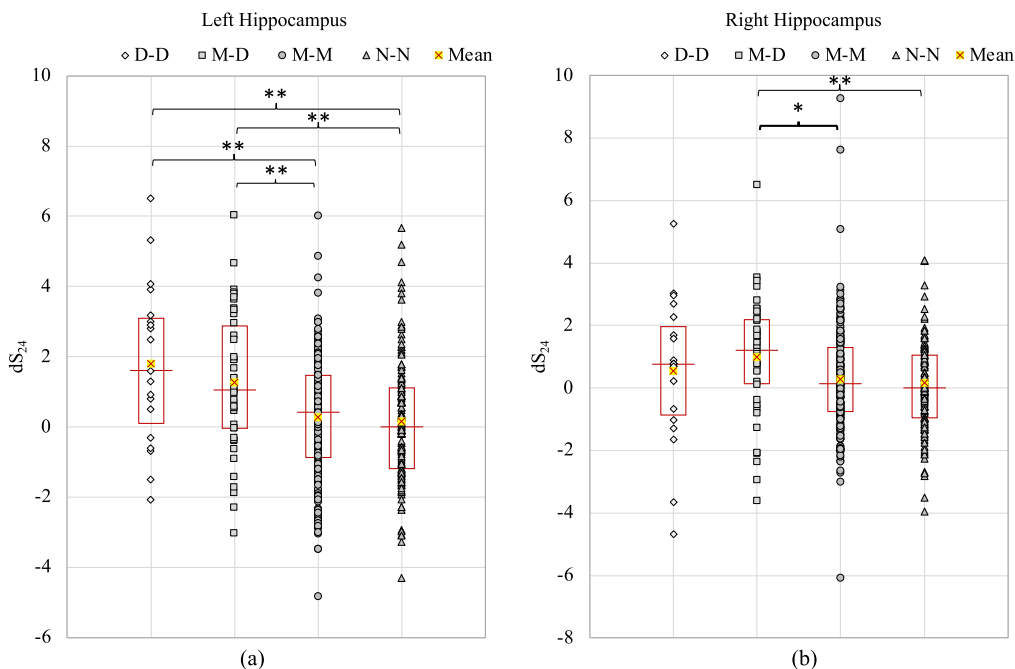


**FIGURE 5** The distributions of shape changes over 24 months ( $dS_{24}$ ) in the left (a) and right (b) hippocampi for each group. Groups are categorized by the changes of cognitive conditions over 24 months with N = normal, M = mild cognitive impairment, and D = dementia. Significant pair-wise comparisons are indicated: \*significant ( $p < .05$ ) and \*\* highly significant ( $p < .01$ )

and M–M, and between Groups M–D and D–D. For the right hippocampus, significant differences were only found between Groups N–N and M–D and between Groups M–M and M–D (Table 4, Figure 5). Further ANCOVA demonstrated significant associations between the  $S_{24}$  of the left and right hippocampus and group category, age, as well as  $S_0$ , but not sex, ApoE4 status, baseline brain amyloid level, and baseline CSF TAU and PTAU concentrations (Table 5).

## 4 | DISCUSSION

In this study, we used 3DZMs to characterize hippocampus shape features and shape changes over 24 months in 428 older adults, including subjects with normal cognition, MCI, and clinical diagnosis of AD dementia. We found significant overall correlations between volume and shape changes over 24 months for both left and right hippocampi. These correlations were mainly driven by the N–N and M–M groups, in which the hippocampus volume reductions were relatively slow (Table 2). These results suggest that at a slower rate of hippocampal volume reduction, changes in both volume and shape occur in a correlated manner. However, in conditions of higher rates of volume reductions, such as in the M–D and D–D groups, the changes in volume and shape no longer remain in correlation. Because the M–N group contains only 10 subjects in this study, this group is too small to be

conclusive regarding the relationship between hippocampal volume and shape changes.

Overall, the shapes of the left and right hippocampi in older subjects changed at a similar pace. However, these trends did not hold across all cognitive conditions. In the M–D group, hippocampal volume reductions occurred at relatively fast rates,  $-7.99 \pm 6.02\%$  for the left and  $-8.46 \pm 5.98\%$  for the right hippocampi (Table 2). Correspondingly, the shapes of the left and right hippocampi also changed at a rapid pace (Table 2) and the shape changes of the left and right hippocampi were correlated to each other (Table 3). In the D–D group, where hippocampal volume reductions also occurred fast,  $-8.79 \pm 8.45\%$  for the left and  $-9.12 \pm 6.31\%$  for the right hippocampus (Table 2). However, the shape of the right hippocampus changed more than that of the left hippocampus (a mean of 10.0% vs. 2.96%) and their changes were not found significantly correlated to each other anymore (Table 3). Overall, the left and right hippocampi appear to change their shapes in a similar magnitude until the subject reaches a state of dementia.

ANOVA demonstrated that shape changes were significantly higher in the D–D and M–D groups compared to the N–N and M–M groups. The volume changes of the N–N and M–M groups were also less than half of the M–D and D–D groups (Table 2). These results suggest that both the hippocampal shape and volume were quite stable in the N–N and M–M groups. ANCOVA further demonstrated that

**TABLE 3** The correlations between the shapes of left and right hippocampi over 24 months

Group	$r, p, CI_{0.95}$		
	$S_0$	$S_{24}$	$dS_{24}$
N–N	0.286, <b><math>7.14 \times 10^{-4}</math></b> , [0.125, 0.465]	0.218, <b>.011</b> , [0.052, 0.392]	0.110, .204, [–0.060, 0.280]
N–M	0.396, .144, [–0.147, 0.984]	0.448, .094, [–0.084, 1.047]	–0.038, .893, [–0.604, 0.528]
M–N	–0.221, .539, [–0.966, 0.516]	–0.373, .289, [–1.132, 0.349]	0.220, .542, [–0.517, 0.964]
M–M	0.377, <b><math>2.35 \times 10^{-8}</math></b> , [0.259, 0.534]	0.582, <b><math>4.22 \times 10^{-20}</math></b> , [0.529, 0.804]	0.213, <b><math>2.14 \times 10^{-3}</math></b> , [–0.078, 0.354]
M–D	0.517, <b><math>4.57 \times 10^{-4}</math></b> , [0.258, 0.886]	0.679, <b><math>7.58 \times 10^{-7}</math></b> , [0.514, 1.142]	0.497, <b><math>8.20 \times 10^{-4}</math></b> , [0.231, 0.859]
D–D	0.301, .211, [–0.180, 0.800]	0.618, <b><math>4.77 \times 10^{-3}</math></b> , [0.232, 1.212]	0.445, .056, [–0.012, 0.968]
Overall	0.457, <b><math>1.98 \times 10^{-23}</math></b> , [0.398, 0.588]	0.572, <b><math>1.33 \times 10^{-38}</math></b> , [0.556, 0.746]	0.226, <b><math>2.43 \times 10^{-6}</math></b> , [0.134, 0.325]

Note:  $S_x$  denotes the Euclidean distance between the shape feature of the hippocampus measured at Month  $x$  and the template.

$dS_{24} = S_{24} - S_0$ .  $r$  = the correlation coefficient between the left and right hippocampi.

$CI_{0.95}$  denotes the 95% confidence interval on the Fisher's  $Z$  value of  $r$ . Significance ones are highlighted in bold.

**TABLE 4** Compare the hippocampus shape changes over 24 months between groups

Between groups	Left hippocampus		Right hippocampus	
	$t$ Value	$p$	$t$ Value	$p$
N–N vs. M–M	.70	.4818	.61	.5449
N–N vs. M–D	3.48	$6.31 \times 10^{-4**}$	2.65	$8.88 \times 10^{-3**}$
N–N vs. D–D	3.68	$3.24 \times 10^{-4**}$	.89	.3732
M–M vs. M–D	3.29	$1.15 \times 10^{-3**}$	2.48	.0137*
M–M vs. D–D	3.57	$4.21 \times 10^{-4**}$	.69	.4930
M–D vs. D–D	.91	.3668	.76	.4518

\*Significant ( $p < .05$ ), \*\*Highly significant ( $p < .01$ ).

**TABLE 5** The effects of cognitive group, sex, age, baseline shape, ApoE4, brain amyloid, cerebrospinal fluid (CSF) TAU, and CSF PTAU on hippocampus shape over 24 months

	Left hippocampus				Right hippocampus			
	SS	DF	F value	p	SS	DF	F value	p
C Group	$4.990 \times 10^{-2}$	3	7.392	$8.09 \times 10^{-5***}$	$3.841 \times 10^{-2}$	3	2.767	$4.169 \times 10^{-2*}$
Sex	$1.000 \times 10^{-5}$	1	.005	.945	$2.000 \times 10^{-5}$	1	.005	.943
Age	$2.941 \times 10^{-2}$	1	13.070	$3.428 \times 10^{-4***}$	$5.758 \times 10^{-2}$	1	12.447	$4.729 \times 10^{-4***}$
S0	1.226	1	544.736	$< 2.20 \times 10^{-16***}$	1.647	1	356.107	$< 2.20 \times 10^{-16***}$
ApoE4 status	$5.610 \times 10^{-3}$	1	2.494	.115	$1.685 \times 10^{-2}$	1	3.644	.0571
Brain amyloid	$6.100 \times 10^{-4}$	1	.269	.604	$4.700 \times 10^{-4}$	1	.102	.750
CSF TAU	$3.000 \times 10^{-4}$	1	.015	.902	$4.000 \times 10^{-5}$	1	.009	.924
CSF PTAU	0.000	1	$6.0 \times 10^{-4}$	.980	.000	1	$2.0 \times 10^{-4}$	.988

Note: C Group = cognitive group N-N, M-M, M-D, and D-D; DF = degree of freedom; S0 = shape at baseline, SS = sum of square.

ApoE4 status: 0 (negative) or 1 (positive with 1 or 2 alleles).

Brain amyloid: Average AV45 SUVR of frontal, anterior cingulate, precuneus, and parietal cortex relative to the cerebellum at baseline.

CSF TAU and PTAU: TAU and PTAU proteins measured in CSF at baseline.

All noncategory inputs (age, S0, amyloid, TAU, and PTAU) had a min-max normalization before statistical analysis.

\*Significant ( $p < .05$ ). \*\*Significant ( $p < .001$ ).

hippocampal shape at Month 24 is significantly associated with the group category, age, and baseline shape, but not with sex. These findings suggest that disease conditions and age likely influence longitudinal hippocampal shape changes, consistent with the observations discussed above. Overall significant correlations between the baseline brain amyloid level and hippocampus shape change over 24 months were found, but not within individual groups. Significant correlations between CSF TAU/PTAU concentration and the shape change were not found. Our ANCOVA analyses did not find significant influence on the hippocampus shape change by ApoE4 status, baseline brain amyloid level, and baseline CSF TAU and PTAU concentrations. Given the exploratory nature of these simple correlation analyses, the relationship between changes in hippocampus shape and the established AD biomarkers remains to be further evaluated.

To improve 3DZM computation efficiency and stability over previous approaches (Canterakis, 1999; Hosny & Hafez, 2012), we have applied the following strategies: For better computational stability, we applied recursive approaches in both spherical harmonics and radial polynomials (Deng & Gwo, 2020). For better computational efficiency, we elected a ZM order of 200 to achieve a high level of accuracy without exceeding available computational resources. We might be able to further reduce the ZM order with a small compromise on the reconstruction accuracy to achieve the goal of characterization of hippocampus shape features. For example, at ZM order of 100, the left and right hippocampus reconstruction error rates of the total 428 subjects at baseline were  $(9.26 \pm 1.47) \times 10^{-2}$  and  $(9.10 \pm 1.35) \times 10^{-2}$ , respectively, which may be sufficient to differentiate shape differences among the disease groups in this study. The second strategy was to apply PCA to reduce the dimension of the ZM descriptor from 10,201 to a much more manageable 120. To confirm the validity of choosing 120 principal components to reduce the dimension of the ZM descriptor, we repeated the above analyses with 30 principal components (expected to contain >80% of the total accumulative

variance), equivalently a 30-dimension ZM descriptor. The overall conclusion was not changed, but the levels of significance in statistical comparisons were reduced. This verification also implies the validity of our dimension reduction strategy to improve computation efficiency in handling large 3D Zernike transformed data sets. Zernike transformation, similar to Fourier transformation, is a general mathematical approach that can be used to quantify the overall shape features as well as the image signal intensity of a complicated object. However, besides the potential challenges in computational efficiency and stability, this approach has limitations in representing specific portions of an object although it still may reveal regional shape changes of an object (Figure 4). The subject distribution also posed limitation on some analyses. While there are 428 subjects in this study, the distribution is heavily tilted to two of the four groups (the N-N and M-M groups), and thus making classification analysis such as support vector machines inappropriate. The D-D group has the smallest size of 19. To further address the effect of the large difference in group sizes on our results, for the four groups we carried comparisons on, we randomly selected 19 subjects in each of the other three groups, and re-ran the between-group comparisons on shape changes (Table 4). We ran 100 trials. For the significant findings in Table 4, while we could not find significance for every trial, as expected, we did find large numbers of trials (25–81 for the highly significant ones and 15 for the significant one) reaching significance. Overall, we have confidence in the results we have reached.

In this study, we demonstrated the applicability of using 3D Zernike transformation to characterize hippocampus shape features in older adults who have different cognitive conditions. We found that the shape of both the left and right hippocampi changed slowly in cognitively normal older adults and patients with MCI and that shape changes were correlated with changes in hippocampal volume under these conditions. However, when a clinical diagnosis of AD dementia occurs, both volume and shape changes of the hippocampus appear

to be accelerated and changes in shape and volume were no longer correlated. Interestingly, we also found that hippocampal shrinkage appeared to occur mainly in the central region in the N–N and M–M groups while it may enlarge at the hippocampal tails and shrink in the central region in the M–D and D–D groups. This observation may suggest the presence of region-specific neurobiological mechanisms underlying the hippocampal shape and volume changes associated with clinical AD progression. Finally, the magnitude of hippocampus shape change was associated with age and disease conditions further suggesting that hippocampal shape features may reveal the underlying neurodegenerative process of clinical AD dementia.

## 5 | CONCLUSION

Taken together, this study represents the first attempt to apply 3D Zernike transformation to characterize the shape and shape changes of the hippocampus over the time course of clinical AD. The findings of this study suggest that the characterization of hippocampus shape features may serve as a novel imaging marker to monitor clinical AD progression and reveal the underlying neurobiology associated with hippocampal volume reduction in older adults.

## ACKNOWLEDGMENTS

This work was partially supported by the National Institutes of Health grant R01AG057571. Data collection and sharing for this project were funded by the Alzheimer's Disease Neuroimaging Initiative (ADNI) (National Institutes of Health grant U01 AG024904) and DOD ADNI (Department of Defense award number W81XWH-12-2-0012). ADNI is funded by the National Institute on Aging, the National Institute of Biomedical Imaging and Bioengineering, and through generous contributions from the following: AbbVie, Alzheimer's Association, Alzheimer's Drug Discovery Foundation, Araclon Biotech, BioClinica, Inc., Biogen, Bristol-Myers Squibb Company, CereSpir, Inc., Cogstate, Eisai Inc., Elan Pharmaceuticals, Inc., Eli Lilly and Company, EuroImmun, F. Hoffmann-La Roche Ltd and its affiliated company Genentech, Inc., Fujirebio; GE Healthcare, IXICO Ltd., Janssen Alzheimer Immunotherapy Research & Development, LLC., Johnson & Johnson Pharmaceutical Research & Development LLC., Lumosity, Lundbeck, Merck & Co., Inc., Meso Scale Diagnostics, LLC., NeuroRx Research, Neurotrack Technologies, Novartis Pharmaceuticals Corporation, Pfizer Inc., Piramal Imaging, Servier, Takeda Pharmaceutical Company, and Transition Therapeutics. The Canadian Institutes of Health Research is providing funds to support ADNI clinical sites in Canada. Private sector contributions are facilitated by the Foundation for the National Institutes of Health ([www.fnih.org](http://www.fnih.org)). The grantee organization is the Northern California Institute for Research and Education, and the study is coordinated by the Alzheimer's Therapeutic Research Institute at the University of Southern California. ADNI data are disseminated by the Laboratory for Neuro Imaging at the University of Southern California.

## DATA AVAILABILITY STATEMENT

Data used in preparation of this article were obtained from the Alzheimer's Disease Neuroimaging Initiative (ADNI) database ([adni.loni.usc.edu](http://adni.loni.usc.edu)).

As such, the investigators within the ADNI contributed to the design and implementation of ADNI and/or provided data but did not participate in analysis or writing of this report.

## ORCID

David C. Zhu  <https://orcid.org/0000-0002-5264-0144>

Chih-Ying Gwo  <https://orcid.org/0000-0002-0678-1966>

## REFERENCES

- Besl, P. J., & McKay, N. D. (1992). Method for registration of 3-D shapes. In P. S. Schenker (Ed.), *Sensor fusion IV: Control paradigms and data structures*. (Vol. 1611, pp. 586–606). Proc. SPIE 1611. <http://proceedings.spiedigitallibrary.org/proceeding.aspx?articleid=981454>
- Canterakis N (1999). 3D Zernike moments and Zernike affine invariants for 3D image analysis and recognition. 11th Scand Conf Image Anal In 11th Sc:85–93. <http://ukpmc.ac.uk/abstract/CIT/504643>.
- Chen, Y., & Medioni, G. (1992). Object modelling by registration of multiple range images. *Image and Vision Computing*, 10, 145–155. <https://linkinghub.elsevier.com/retrieve/pii/026288569290066C>
- Daberdaku, S., & Ferrari, C. (2018). Exploring the potential of 3D Zernike descriptors and SVM for protein–protein interface prediction. *BMC Bioinformatics*, 19, 35. <https://bmcbioinformatics.biomedcentral.com/articles/10.1186/s12859-018-2043-3>
- Deng, A.-W., & Gwo, C.-Y. (2018). Efficient computations for generalized Zernike moments and image recovery. *Applied Mathematics and Computation*, 339, 308–322. <https://linkinghub.elsevier.com/retrieve/pii/S0096300318305873>
- Deng, A.-W., & Gwo, C.-Y. (2020). A stable algorithm computing high-order 3D Zernike moments and shape reconstructions. In *Proceedings of the 2020 4th international conference on digital signal processing* (pp. 38–42). ACM. <https://dl.acm.org/doi/10.1145/3408127.3408130>
- Fischl, B., Salat, D. H., Busa, E., Albert, M., Dieterich, M., Haselgrove, C., van der Kouwe, A., Killiany, R., Kennedy, D., Klaveness, S., Montillo, A., Makris, N., Rosen, B., & Dale, A. M. (2002). Whole brain segmentation: Automated labeling of neuroanatomical structures in the human brain. *Neuron*, 33, 341–355. <http://www.ncbi.nlm.nih.gov/pubmed/11832223>
- Gwo, C.-Y., Zhu, D. C., & Zhang, R. (2019). Brain white matter hyperintensity lesion characterization in T2 fluid-attenuated inversion recovery magnetic resonance images: Shape texture, and potential growth. *Frontiers in Neuroscience*, 13, 353. <https://www.frontiersin.org/article/10.3389/fnins.2019.00353/full>
- Hosny, K. M., & Hafez, M. A. (2012). An algorithm for fast computation of 3D Zernike moments for volumetric images. *Mathematical Problems in Engineering*, 2012, 1–17.
- Jack, C. R., Petersen, R. C., Xu, Y. C., O'Brien, P. C., Smith, G. E., Ivnik, R. J., Boeve, B. F., Waring, S. C., Tangalos, E. G., & Kokmen, E. (1999). Prediction of AD with MRI-based hippocampal volume in mild cognitive impairment. *Neurology*, 52, 1397–1403. <http://www.neurology.org/lookup/doi/10.1212/WNL.52.7.1397>
- Jack, C. R., Shiung, M. M., Gunter, J. L., O'Brien, P. C., Weigand, S. D., Knopman, D. S., Boeve, B. F., Ivnik, R. J., Smith, G. E., Cha, R. H., Tangalos, E. G., & Petersen, R. C. (2004). Comparison of different MRI brain atrophy rate measures with clinical disease progression in AD. *Neurology*, 62, 591–600.
- Jack, C. R., Shiung, M. M., Weigand, S. D., O'Brien, P. C., Gunter, J. L., Boeve, B. F., Knopman, D. S., Smith, G. E., Ivnik, R. J., Tangalos, E. G., & Petersen, R. C. (2005). Brain atrophy rates predict subsequent clinical conversion in normal elderly and amnesic MCI. *Neurology*, 65, 1227–1231.
- Jagust, W. (2013). Vulnerable neural systems and the borderland of brain aging and neurodegeneration. *Neuron*, 77, 219–234. <https://linkinghub.elsevier.com/retrieve/pii/S0896627313000342>

- Khotanzad, A., & Hong, Y. H. (1990). Invariant image recognition by Zernike moments. *IEEE Transactions on Pattern Analysis and Machine Intelligence*, 12, 489–497. <http://ieeexplore.ieee.org/document/55109/>
- Kintner, E. C. (1976). On the mathematical properties of the Zernike polynomials. *Optica Acta: International Journal of Optics*, 23, 679–680. <https://www.tandfonline.com/doi/full/10.1080/713819334>
- Liu, H., Fang, Y., & Huang, Q. (2019). Efficient representation of head-related transfer functions with combination of spherical harmonics and spherical wavelets. *IEEE Access*, 7, 78214–78222.
- McKhann, G. M., Knopman, D. S., Chertkoff, H., Hyman, B. T., Jack, C. R., Kawas, C. H., Klunk, W. E., Koroshetz, W. J., Manly, J. J., Mayeux, R., Mohs, R. C., Morris, J. C., Rossor, M. N., Scheltens, P., Carrillo, M. C., Thies, B., Weintraub, S., & Phelps, C. H. (2011). The diagnosis of dementia due to Alzheimer's disease: Recommendations from the National Institute on Aging-Alzheimer's association workgroups on diagnostic guidelines for Alzheimer's disease. *Alzheimer's & Dementia*, 7, 263–269. <https://doi.org/10.1016/j.jalz.2011.03.005>
- Novotni, M., & Klein, R. (2004). Shape retrieval using 3D Zernike descriptors. *Computer-Aided Design*, 36, 1047–1062.
- Papakostas, G. A., Boutalis, Y. S., Karras, D. A., & Mertzios, B. G. (2007). A new class of Zernike moments for computer vision applications. *Information Sciences*, 177, 2802–2819. <https://linkinghub.elsevier.com/retrieve/pii/S0020025507000394>
- Petersen, R. C., Roberts, R. O., Knopman, D. S., Boeve, B. F., Geda, Y. E., Ivnik, R. J., Smith, G. E., & Jack, C. R. (2009). Mild cognitive impairment: Ten years later. *Archives of Neurology*, 66, 1447–1455. <http://www.ncbi.nlm.nih.gov/pubmed/20008648>
- Petersen, R. C., Smith, G. E., Waring, S. C., Ivnik, R. J., Tangalos, E. G., & Kokmen, E. (1999). Mild cognitive impairment: Clinical characterization and outcome. *Archives of Neurology*, 56, 303–308.
- Pievani, M., Galluzzi, S., Thompson, P. M., Rasser, P. E., Bonetti, M., & Frisoni, G. B. (2011). APOE4 is associated with greater atrophy of the hippocampal formation in Alzheimer's disease. *NeuroImage*, 55, 909–919. <https://linkinghub.elsevier.com/retrieve/pii/S105381191100005X>
- Querfurth, H. W., & LaFerla, F. M. (2010). Alzheimer's disease. *The New England Journal of Medicine*, 362, 329–344. [http://www.ncbi.nlm.nih.gov/entrez/query.fcgi?cmd=Retrieve&db=PubMed&dopt=Citation&list\\_uids=20107219](http://www.ncbi.nlm.nih.gov/entrez/query.fcgi?cmd=Retrieve&db=PubMed&dopt=Citation&list_uids=20107219)
- Styner, M., Oguz, I., Xu, S., Brechbühler, C., Pantazis, D., Levitt, J. J., Shenton, M. E., & Gerig, G. (2006). Framework for the statistical shape analysis of brain structures using SPHARM-PDM. *Insight Journal*, 1071, 242–250. <http://www.ncbi.nlm.nih.gov/pubmed/21941375>
- 0A<http://www.pubmedcentral.nih.gov/articlerender.fcgi?artid=PMC3062073>
- Szegő, G. (1939). *Orthogonal polynomials* (Vol. 23). Colloquium Publications. <http://www.ams.org/coll/023>
- Venkatraman, V., Sael, L., & Kihara, D. (2009). Potential for protein surface shape analysis using spherical harmonics and 3D Zernike descriptors. *Cell Biochemistry and Biophysics*, 54, 23–32. <http://www.ncbi.nlm.nih.gov/pubmed/19521674>
- Wachinger, C., Salat, D. H., Weiner, M., & Reuter, M. (2016). Whole-brain analysis reveals increased neuroanatomical asymmetries in dementia for hippocampus and amygdala. *Brain*, 139, 3253–3266.
- Wang, K., Zhu, T., Gao, Y., & Wang, J. (2019). Efficient terrain matching with 3-D Zernike moments. *IEEE Transactions on Aerospace and Electronic Systems*, 55, 226–235. <https://ieeexplore.ieee.org/document/8395033/>
- Wang, K., Zhu, T., & Wang, J. (2018). Real-time terrain matching based on 3D Zernike moments. *Journal of Navigation*, 71, 1441–1459. [https://www.cambridge.org/core/product/identifier/S0373463318000449/type/journal\\_article](https://www.cambridge.org/core/product/identifier/S0373463318000449/type/journal_article)
- Wee, C.-Y., & Paramesran, R. (2007). On the computational aspects of Zernike moments. *Image and Vision Computing*, 25, 967–980. <https://linkinghub.elsevier.com/retrieve/pii/S0262885606002204>
- Zernike, v. F. (1934). Beugungstheorie des schneidenverfahrens und seiner verbesserten form, der phasenkontrastmethode. *Physica*, 1, 689–704. <https://linkinghub.elsevier.com/retrieve/pii/S0031891434802595>

## SUPPORTING INFORMATION

Additional supporting information can be found online in the Supporting Information section at the end of this article.

**How to cite this article:** Zhu, D. C., Gwo, C.-Y., Deng, A.-W., Scheel, N., Dowling, M. A., Zhang, R., & for the Alzheimer's Disease Neuroimaging Initiative (2023). Hippocampus shape characterization with 3D Zernike transformation in clinical Alzheimer's disease progression. *Human Brain Mapping*, 44(4), 1432–1444. <https://doi.org/10.1002/hbm.26130>